Effects of interleaflet coupling on the morphologies of multicomponent lipid bilayer membranes

Chloe M. Funkhouser, Michael Mayer, Francisco J. Solis, and K. Thornton

Citation: J. Chem. Phys. **138**, 024909 (2013); doi: 10.1063/1.4773856
View online: http://dx.doi.org/10.1063/1.4773856
View Table of Contents: http://jcp.aip.org/resource/1/JCPSA6/v138/i2
Published by the American Institute of Physics.

Effects of interleaflet coupling on the morphologies of multicomponent lipid bilayer membranes

Chloe M. Funkhouser,[1] Michael Mayer,[1,2] Francisco J. Solis,[3] and K. Thornton[4]
[1]*Department of Biomedical Engineering, University of Michigan, Ann Arbor, Michigan 48109, USA*
[2]*Department of Chemical Engineering, University of Michigan, Ann Arbor, Michigan 48109, USA*
[3]*Division of Mathematical and Natural Sciences, Arizona State University, Glendale, Arizona 85306, USA*
[4]*Department of Materials Science and Engineering, University of Michigan, Ann Arbor, Michigan 48109, USA*

(Received 3 July 2012; accepted 14 December 2012; published online 14 January 2013)

We investigate dynamical and stationary compositional and surface morphologies in macroscopically phase-separating multicomponent lipid bilayer membranes using a computational model. We employ a phase-field method for the description of the coexisting phases and treat the two leaflets individually while including interleaflet interactions. The compositional evolution of the two leaflets is coupled to the shape evolution of the membrane via a Helfrich free energy with a composition-dependent spontaneous curvature. We investigate the effects of the interleaflet interaction on the dynamics and stationary states of a system favoring nonzero spontaneous curvatures. Morphological phase diagrams are mapped in composition space using three different interleaflet coupling strengths. We find that characteristics sensitive to the coupling strength include the time required to develop regions of fully separated phases, the prevalence of a stripe morphology, and the shifting of phase compositions to accommodate energetically favorable interactions across leaflets. Characteristics found to be robust with respect to coupling strength include (1) the stripe morphology is favored at nearly equal mixtures and (2) phase separation is prevented in systems where a pair of phases that preferentially interact across leaflets together occupy nearly all or none of the membrane. © *2013 American Institute of Physics*. [http://dx.doi.org/10.1063/1.4773856]

I. INTRODUCTION

Lipid rafts have an important role in numerous cellular processes as well as in the process of infection by certain pathogens.[1–3] Rafts are defined as highly dynamic membrane structures of 10–200 nm in size, enriched in sphingolipids and sterols.[4] Lipid rafts are difficult to study directly in live cells because of their small length scale and short lifetime, and therefore model membrane systems such as planar lipid bilayers and giant unilamellar vesicles are commonly used to study the lipid phase behavior underlying raft formation and dynamics. Model membrane systems composed of ternary lipid mixtures can phase separate to produce domains of liquid-ordered and liquid-disordered phases.[5–8] The liquid-ordered phase has fluidity and molecular order between those of the liquid-disordered and gel states. The plasma membrane of cells can consist of coexisting liquid-disordered and liquid-ordered phases, where lipid rafts are thought to be the latter of these phases. Model membrane systems are useful since phase-separated domains are typically much larger in size (tens of microns) and are therefore resolvable with optical microscopy. While the length and time scales in these model systems may differ from those in cell plasma membranes, much can still be learned about the behavior of lipids in these model systems. Some hypotheses for the differences between the reported size and behavior of domains observed in model membranes and in those believed to exist in cell plasma membranes have been discussed and investigated in Refs. 9–13, which include the absence of proteins and a cytoskeleton in the model membrane systems.

The plasma membrane of cells has an asymmetric composition, meaning that different lipid species are found in the inner (cytoplasmic) and outer (extracellular) leaflets. The inner leaflet tends to be rich in phosphatidylserine and phosphatidylethanolamine, while the outer leaflet tends to be rich in phosphatidylcholine and sphingomyelin.[14–17] In model membranes composed of a lipid mixture similar to common inner leaflets, phase separation is typically not observed.[18] However, the opposite is true in model membranes composed of mixtures similar to those of outer leaflets, where phase separation is observed for a variety of different mixtures.[19,20] These results from model membranes are thought to translate to lipid rafts in living cell membranes. To our knowledge, no studies have been conducted to date to investigate alignment and interaction of lipid rafts across the leaflets in the plasma membrane of a living cell.

There is theoretical and experimental evidence[21–23] that the phase behavior of one leaflet can influence the behavior of the opposing leaflet. In asymmetric planar lipid bilayer membranes composed of simple mixtures to mimic the inner and outer leaflets of a cell plasma membrane, Collins and Keller found that phase separation can be induced in the inner leaflet (or can be suppressed in the outer leaflet), depending on the strength of the tendencies of the leaflets to phase separate (or to remain homogeneous).[20] It has also been observed that in model membranes where both leaflets phase separate, the domains in the two leaflets interact and tend to align laterally.[24,25] Interleaflet interactions can in some cases introduce additional phases that would not be present

in the absence of such interactions, where three different fluorescence intensities corresponding to three phases in a single leaflet (rather than the expected two phases) have been observed.[20] Estimates of the strength of this interleaflet coupling have been reported from studies employing a molecular mean-field model[26] and a coarse-grained simulation model.[27]

As an example of a process in living cells where there is evidence that interleaflet coupling plays an important role, it has been observed that peripheral proteins (interacting with only one leaflet of the membrane) can "sense" the presence of peripheral proteins interacting with the opposite leaflet to trigger signaling cascades. In some cases, transmembrane proteins assist in this "sensing" by interacting with both peripheral proteins, but in other cases the "sensing" is thought to occur via the membrane lipids alone.[13,28–31] In the latter case, it is hypothesized that specific lipids in the outer leaflet first cluster around a peripheral protein, inducing lipids to cluster at the same location in the inner leaflet, which then in turn attracts the second peripheral protein to the inner leaflet.[31]

Mechanisms to explain this transmembrane lipid coupling have been proposed, although the dominant effect has not been fully determined. These mechanisms include interdigitation of the tailgroups of the lipids in the opposing leaflets,[32] the exchange of cholesterol across the bilayer, and molecule-molecule interactions similar to what liquid-disordered and liquid-ordered phases in a single leaflet experience at their interface.[33,34] Spontaneous flip-flop of lipids from one leaflet to the other can occur, but typically on time scales much longer than the coupling observed in experiments due to the energetic penalty of bringing a hydrophilic lipid headgroup through the hydrophobic tail region of the bilayer.

Spontaneous curvature is a characteristic of membrane systems where the effective molecular shapes of the membrane components give the membrane a tendency to adopt a particular curved morphology. The effective molecular shape of a lipid is a function of not only its physical dimensions but can also be affected by other factors that influence its packing with other lipids, such as electrostatic attraction and repulsion. One example of a lipid membrane with nonzero spontaneous curvature is a single-component lipid monolayer with a lipid headgroup that occupies a different area in the plane of the membrane than the tailgroup. Another example is an asymmetric bilayer, where nonzero spontaneous curvature can arise if the dimensions of the lipids in the two leaflets differ. For a single-component (and therefore symmetric) lipid bilayer, the dimensions of the lipids in the two opposing leaflets are the same, and the membrane would therefore have zero spontaneous curvature. It has been shown that phases that appear in lipid membrane systems can affect the shape of the membrane, and that the shape of the membrane can affect the morphologies of the phases.[7,8,35–37] However, in these studies the membranes were produced such that the two leaflets were composed of the same lipids, and there was also no evidence that like-phases were not in registration, which would be required to produce nonzero spontaneous curvatures. Other aspects of the membrane composition can influence the shape, including the line-tension energy, excess area, and bending rigidity. In asymmetric membrane systems, where nonzero spontaneous curvatures can arise,[38–42] the bending energy associated with spontaneous curvatures adds an additional element to the coupling between membrane composition and shape.

Numerous theoretical and computational studies of membrane phase separation, often coupled with deformation, have been undertaken. Continuum-level computational studies coupling membrane shape with compositional domains have been performed in two dimensions with the effects of hydrodynamic flow,[43] and in three dimensions both excluding[44,45] and including[46–48] spontaneous curvature effects. The model presented by Sample and Golovin applies to double membranes such as those in some intracellular organelles, and includes an interaction term to couple the two membranes that have differing compositions,[47] while Khelashvili, Harries, and Weinstein considered the two leaflets of a bilayer membrane, where the spontaneous curvature of each of the leaflets is included in the free energy individually.[48] Mean-field morphological phase diagrams for coupled bilayers in the absence of mechanical effects were produced by Hirose, Komura, and Andelman, imposing an energetic penalty when dissimilar species align across the bilayer.[49] Kumar, Gompper, and Lipowsky also produced morphological phase diagrams for two-component bilayers and three-component monolayer membranes in the weak segregation limit, including spontaneous curvature effects.[50] They found that the two-component bilayers and three-component monolayers exhibited similar phase behavior.

In this work, we model macroscopic phase separation in the two leaflets of a nearly planar lipid bilayer membrane using a continuum-level model, coupling the leaflet compositions to mechanical properties of the membrane phases. The leaflets have different compositions, but we specify that both leaflets adopt the same shape profile since they together form a bilayer (i.e., the two leaflets cannot adopt different shapes since they must compose a single, cohesive bilayer structure). Rather than assigning a separate spontaneous curvature to each monolayer as in Ref. 48, we compute the composition-dependent spontaneous curvature of the bilayer as a whole based on a simple geometrical model. We simulate the evolution of the composition and the shape of asymmetric membranes, governed by a competition between the line-tension, bending, and surface-tension energies, as well as an energy dictating the coupling between the two leaflets of the bilayer. The line tension arises from the interfaces between coexisting thermodynamic phases, which have excess energy; this contribution to the total free energy is decreased when the total length of interfaces is reduced. The bending energy arises from the membrane's resistance to bending away from its spontaneous configuration; this energy is minimized when phases are able to adopt this spontaneous curvature. Surface-tension energy arises from the largely conserved surface area of the membrane and is minimized by a perfectly planar membrane.

The interleaflet coupling energy reflects the molecular interactions between the tail groups of the two leaflets, which determine which phases prefer to co-occupy a position on the membrane on the opposing leaflets. Since the focus of the work presented here is on the effects of nonzero spontaneous curvature, we specify that the lipids in the two leaflets

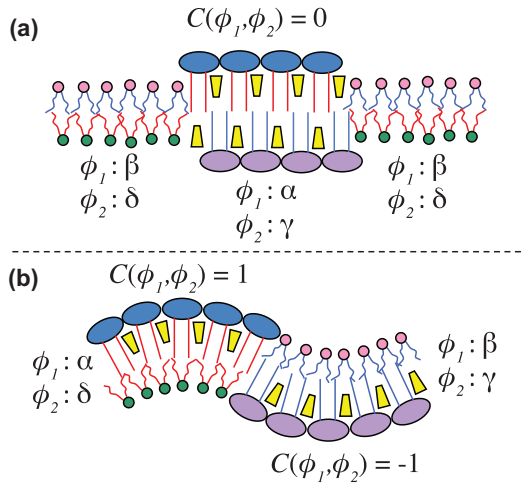

FIG. 1. Bilayer configurations and their spontaneous curvatures. The interaction energy H_3 specifies that the configuration shown in (a) with zero spontaneous curvature is set to have higher energy than that in (b) with nonzero spontaneous curvature. The schematics illustrate how, as a result of the different lengths of the tailgroups in the phases, hydrophobic forces could favor the configurations in (b) over (a) since the bilayer is more cohesive.

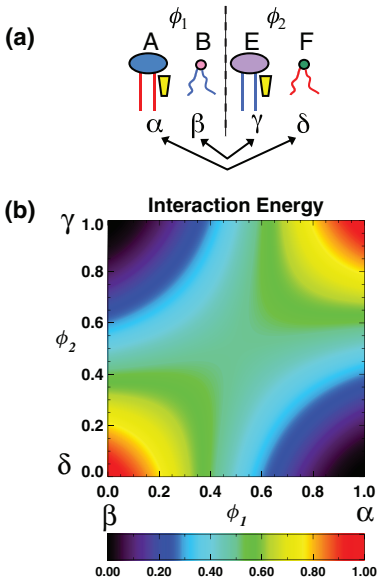

FIG. 2. (a) Schematics of the molecules composing the two leaflets and the phases that they tend to partition into. The α and γ phases are rich in components A and E, respectively, and the third component that is not explicitly tracked in our pseudobinary model. This third component is illustrated to represent cholesterol, since it largely partitions with saturated lipids (A and E). The tailgroup colors and the arrows indicate which components prefer to interact. (b) Color contour plot of H_3, the interleaflet interaction energy, with respect to the compositional phase-fields ϕ_1 and ϕ_2. The locations of the minima and maxima determine which phases (represented by the phase-field values) have preferred and non-preferred interactions.

interact with each other across the bilayer such that lipid arrangements leading to nonzero spontaneous curvatures are energetically favored over those leading to zero spontaneous curvature. While such "anti-registration" of like-phases giving rise to nonzero spontaneous curvatures is thought to be atypical, it was observed in Refs. 51 and 52. In these studies, a difference in the length of the lipid tailgroups made anti-registration configurations favorable, likely as a result of the hydrophobic effect, which entropically favors a cohesive bilayer. This mechanism is illustrated in Fig. 1, where a more cohesive bilayer is produced when like-domains are in anti-registration. The interleaflet coupling term in the model collectively represents interaction mechanisms such as the hydrophobic effect, as well as hypothesized mechanisms for interleaflet "communication" such as cholesterol flip-flop. This consideration of the mechanical properties of lipids differentiates our works from that of Hirose *et al.*[49] where no mechanical effects were included, and hence the sign of the coupling term was irrelevant.

II. BILAYER MODEL

A. Phase-field modeling

In this bilayer model each of the two leaftlets is treated individually using two scaled composition variables, ϕ_1 and ϕ_2. Each leaflet is modeled as a ternary system (representing, for example, a saturated lipid, an unsaturated lipid, and cholesterol). However, in the model, the composition of each leaflet is a pseudobinary representation of this ternary system; the composition variables ϕ_1 and ϕ_2 represent the composition along a line drawn across the phase transformation path of the ternary phase diagram. At any position on this line, there is a mixture of three components, although by taking this slice we can specify the composition in this model in terms of just two components. We model leaflet 1 to be composed of species A and B, while leaflet 2 is composed of species E and F. The α and β phases exist in leaflet 1, rich in components A and B, respectively; the γ and δ phases exist in leaflet 2, rich in components E and F, respectively. A schematic illustration of the shapes of species in the two leaflets is given in Fig. 2(a). Phase separation is described using a phase-field model, with ϕ_1 and ϕ_2 serving as the phase fields in the two leaflets. ϕ_1 and ϕ_2 are related to the concentrations of components A and E by

$$\phi_1 = \frac{c^A - c^A_\beta}{c^A_\alpha - c^A_\beta}, \quad \phi_2 = \frac{c^E - c^E_\delta}{c^E_\gamma - c^E_\delta}, \tag{1}$$

where c^A_α specifies the concentration of species A in the α phase. This definition dictates that $\phi_1 = 1$ in the α phase and $\phi_1 = 0$ in the β phase, while $\phi_2 = 1$ in the γ phase and $\phi_2 = 0$ in the δ phase. We choose the equilibrium concentrations to be $c^A_\alpha = c^E_\gamma = 0.8$ and $c^A_\beta = c^E_\delta = 0.2$ to approximate the compositions of the liquid-ordered and liquid-disordered phases in ternary membrane systems below their miscibility transition temperature.[53] We note that in some simulations, the minimum and maximum values of the composition variables ϕ_1 and ϕ_2 reach values outside of [0, 1] by as much as ± 0.25, corresponding to concentrations of c^A, $c^E = 0.05$ and 0.95.

B. Free energy

The total free energy in the model is defined by a sum of four terms:

$$F = \int H dA = \int (H_0 + H_1 + H_2 + H_3) dA. \tag{2}$$

The first energy density, H_0, describes the thermodynamics of the mixture in each leaflet $p = 1, 2$:

$$H_0 = \sum_{p=1}^{2} \left[\frac{w}{4}\phi_p^2(1-\phi_p)^2 + \frac{\zeta^2}{2}\nabla^i\phi_p\nabla_i\phi_p \right], \quad (3)$$

where w defines the barrier height in the double-well free energy and ζ sets the energetic penalty for composition gradients. The model is used only in the strong segregation regime, where, for flat systems, the line tension of a straight phase boundary can be identified with $\lambda = (w\zeta^2/72)^{1/2}$. We use the standard notation of superindices and subindices for contravariant and covariant vectors, respectively, as well as the repeated index summation convention as shown in the notation of the gradient term. These indices identify generalized coordinates that parametrize the surface. All spatial derivative operators are taken along the deformed membrane surface; explicit expressions for these differential operators are derived in covariant form similar to the manner described in previous work of our group.[54] While different parameters could be used in this energy density for the individual leaflets, we use identical parameters in order to isolate and focus on the effects of interleaflet coupling.

The second energy density is a modified Helfrich Hamiltonian[55] describing the mechanical properties of the membrane, coupling compositions, and the membrane shape:

$$H_1 = \frac{\Lambda}{2}(K - C(\phi_1, \phi_2))^2. \quad (4)$$

In this expression, Λ is the membrane bending rigidity, K is the trace of the curvature tensor and is equal to twice the mean curvature, and $C(\phi_1, \phi_2)$ is the spontaneous curvature defined as a function of the two compositions in the leaflets, as discussed in Sec. II C.

The third contribution to the energy density controls the total area of the membrane and is given by a surface tension:

$$H_2 = \sigma. \quad (5)$$

The tension σ is an isotropic contribution to the stress tensor that opposes an increase in the membrane area. This term arises from a coarse-graining of cohesive forces between the molecules that form the membrane. While its origin is physical, surface tension can also be viewed mathematically as the Lagrange multiplier for area used to penalize changes in area. Upon integration of this density, we obtain a linear coupling of the tension and the total area of the membrane, A.

Lastly, the fourth term in the free energy, H_3, models the coupling between bilayer leaflets and is a function of the two leaflet compositions, scaled with the coupling strength χ:

$$H_3 = \frac{\chi}{2}[(\phi_1 + \phi_2 - 1)^2 + ((\phi_1 - \phi_2)^2 - 1)^2]. \quad (6)$$

A contour plot of H_3 in (ϕ_1, ϕ_2) space is presented in Fig. 2(b), where the locations of valleys determine which phases prefer to align across the two leaflets of the bilayer. As schematically indicated by the arrows in Fig. 2(a), the phases that prefer to colocate across the leaflets as defined by H_3 are rich in species with different headgroup sizes, which produces nonzero spontaneous curvatures. The magnitude of χ determines how strong the coupling between leaflets is, with larger values imposing greater energetic penalties for non-preferred interactions across the leaflets.

C. Relating composition to spontaneous curvature

The spontaneous curvature appearing in the free energy contribution H_1 is defined as a function of the compositions in each leaflet. Since the spontaneous curvature is a property stemming from the shapes of the lipid molecules in the two leaflets, we introduce an intermediate variable in each leaflet: the effective headgroup diameter of the lipid species denoted as D. This variable is taken to be a function of the local composition and relates the spontaneous curvature to composition through the following geometrical model.

For simplicity, it is assumed that components A and E are similar to each other in geometry, as are B and F (but different from A and E) as illustrated in Fig. 2(a). In leaflet 1 at equilibrium, the α phase is rich in species A, while the β phase is rich in species B. Similarly, in leaflet 2 at equilibrium, the γ phase is rich in species E, while the δ phase is rich in species F. The effective headgroup diameter in the α and γ phases is denoted as $d_{\alpha,\gamma}$ and similarly in the β and δ phases as $d_{\beta,\delta}$, with $d_{\alpha,\gamma} > d_{\beta,\delta}$. The function $D_p(\phi_p)$ for each leaflet, $p = 1$ or 2, is defined to smoothly interpolate between its local maximum at $D_p(\phi_p = 1) = d_{\alpha,\gamma}$ and local minimum at $D_p(\phi_p = 0) = d_{\beta,\delta}$ using an interpolation function of the form $f(x) = a(x^2(3 - 2x)) + b$ that ensures that the interpolated value slowly approaches $f(x = 0)$ and $f(x = 1)$ (where the derivative vanishes) and rapidly changes away from these values. Specifically,

$$D_p(\phi_p) = (d_{\alpha,\gamma} - d_{\beta,\delta})\left(\phi_p^2(3 - 2\phi_p)\right) + d_{\beta,\delta}. \quad (7)$$

Since ϕ_1 and ϕ_2 reach values outside of [0, 1] in some simulations, producing an error in the function $D_p(\phi_p)$ of up to 5%, test simulations were performed for cases with extreme values of ϕ_p where both ϕ_1 and ϕ_2 were truncated at [0, 1] for spontaneous curvature calculations. These tests produced results nearly identical in terms of dynamic and stationary phase morphologies to the results presented.

Finally, the spontaneous curvature function, $C(\phi_1, \phi_2)$, can be defined as a function of D in each leaflet, $C(D_1(\phi_1), D_2(\phi_2))$. Using a simple geometric argument based on similar triangles as illustrated in Fig. 3, C is related to the headgroup diameter and the bilayer thickness L by

$$C(D) = \frac{2}{L}\frac{D_1 - D_2}{D_1 + D_2}. \quad (8)$$

To examine the particular effects of nonzero spontaneous curvature, the interaction energy H_3 is set such that the α phase prefers to interact with δ and the β phase prefers γ, as indicated by the arrows in Fig. 2(a). When α is aligned with δ, we define that $C = 1$; when β is aligned with γ, we define that $C = -1$. If α is aligned with γ or if β is aligned with δ, the bilayer is symmetric with respect to molecular shapes, and these configurations are therefore assigned to have $C = 0$. These configurations are illustrated in Fig. 1. Spontaneous curvature values of $C = 1$ and $C = -1$ represent curvatures of $(20\ \text{nm})^{-1}$ and $(-20\ \text{nm})^{-1}$, respectively, with a bilayer thickness of $L = 3.6$ nm.[56,57] The headgroup diameters $d_{\alpha,\gamma}$ and

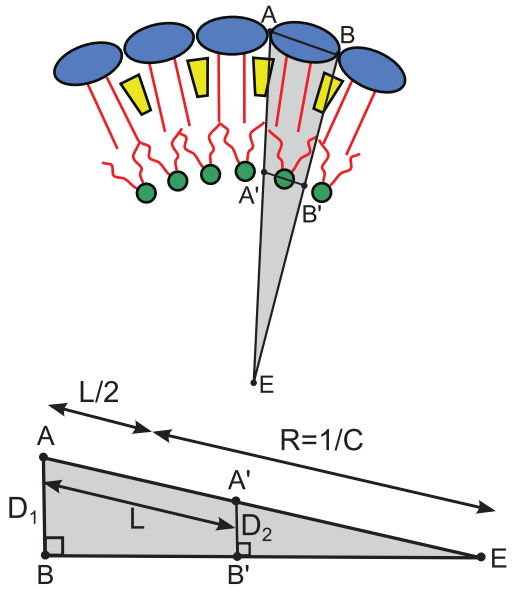

FIG. 3. Schematic of the relationship between spontaneous curvature C, headgroup diameters D_1 and D_2, and bilayer thickness L used to derive Eq. (8). Triangles ABE and $A'B'E$ are geometrically similar.

$d_{\beta,\delta}$ are representative of a generic system with mismatched lipid headgroup sizes, rather than tuned to a specific system of lipids.

D. Shape deformations and dynamics

The most general (small) shape deformation of the membrane is a composite of tangential and normal deformations. It should be noted that while the two leaflets can differ in composition, they are assumed to maintain a constant separation distance even during deformations, and therefore the membrane possesses only a single shape adopted by the two leaflets together. As in our previous model, which is similar but does not consider interleaflet interactions,[54] the normal deformations can be written as $\delta\mathbf{x} = \psi\mathbf{n}$ where ψ is the deformation scalar and $\mathbf{n}$ is the normal unit vector. For a multicomponent membrane, tangential deformations advect the composition field and induce internal changes in composition. However, the resulting compositional evolution can be reformulated into a combination of normal deformations and compositional redistribution (i.e., advection) as described in Ref. 58. It is therefore possible to describe the dynamics, including tangential flows, by accounting for normal deformations, diffusion processes, and compositional advection. The free energy change associated with a normal deformation $\psi\mathbf{n}$ can be written as the integral $\delta F = -\int T\psi\, dA$, where T is the generalized force density that couples to the displacement ψ. The normal velocity field is $\mathbf{v}_n = \partial_t\psi\mathbf{n}$, and the friction force opposing the motion is $\mathbf{f}_v = -\mathbf{v}_n/\Gamma = -\partial_t\psi\mathbf{n}/\Gamma$, where Γ is the inverse of the friction coefficient. The dynamical equation is then obtained from the condition $T\mathbf{n} + \mathbf{f}_v = \mathbf{0}$:

$$\frac{\partial\psi}{\partial t} = \Gamma T, \tag{9}$$

$$-T = HK + \Lambda(K - C)(R - K^2) - \Lambda\Delta(K - C) - \zeta^2 K^{ab}\nabla_a\phi\nabla_b\phi, \tag{10}$$

where R is the scalar curvature equal to the determinant of the curvature tensor, Δ is the Laplace operator, and K^{ab} is the curvature tensor (see Ref. 54 for derivations).

We use a Cahn-Hilliard-type dynamics for the composition of each leaflet denoted by $p = 1, 2$, where $\mu_p = \delta F/\delta\phi_p$ is the chemical potential for the dimensionless composition, ϕ_p, of leaflet p. Equilibrium is achieved when the chemical potential becomes uniform so that its gradient is zero. The dynamics is described by an evolution equation,

$$\frac{\partial\phi_p}{\partial t} = M\Delta\mu_p, \tag{11}$$

$$\mu_1 = \frac{w}{2}\phi_1(1-\phi_1)(1-2\phi_1) - \zeta^2\Delta\phi_1 + \Lambda\frac{\delta C}{\delta\phi_1}[C(\phi_1,\phi_2) - K] + \chi[\phi_1 + \phi_2 - 1 + 2((\phi_1 - \phi_2)^2 - 1)(\phi_1 - \phi_2)], \tag{12}$$

$$\mu_2 = \frac{w}{2}\phi_2(1-\phi_2)(1-2\phi_2) - \zeta^2\Delta\phi_2 + \Lambda\frac{\delta C}{\delta\phi_2}[C(\phi_1,\phi_2) - K] + \chi[\phi_1 + \phi_2 - 1 - 2((\phi_1 - \phi_2)^2 - 1)(\phi_1 - \phi_2)], \tag{13}$$

where

$$\frac{\delta C}{\delta\phi_1} = \frac{2}{L}\frac{dD_1}{d\phi_1}\left(\frac{1}{D_1 + D_2} - D_1(D_1 + D_2)\right), \tag{14}$$

$$\frac{\delta C}{\delta\phi_2} = \frac{2}{L}\frac{dD_2}{d\phi_2}\left(\frac{1}{D_1 + D_2} - D_2(D_1 + D_2)\right). \tag{15}$$

Note that D_1 and D_2 are functions of ϕ_1 and ϕ_2, respectively. We assume the dynamics of the shape to be that of a single scalar variable. Thus, it is viable to use the Monge gauge, where after setting a fixed planar geometrical background, we describe the shape of a membrane by specifying its position (height) from this projected background and require that this projection be one-to-one. These shapes are then described by a single height function $h(\mathbf{u})$ with respect to a two-dimensional Cartesian coordinate $\mathbf{u}$ that parametrizes the membrane surface. In order to apply our dynamical equations in these coordinates, the normal deformation rate, $\partial\psi/\partial t$, is converted into the height deformation rate, $\partial h/\partial t$. This is accomplished using the relation

$$\frac{\partial h}{\partial t} = \Gamma g^{1/2} T, \tag{16}$$

where g is the area differential.[54]

Finally, the compositions at a point above a fixed location $\mathbf{u}$ in the reference plane change not only due to diffusion but also due to the motion of the surface, which introduces an advection term in the evolution equation for each of the two leaflets $p = 1, 2$:

$$\begin{aligned}\partial_t\phi_p|_{\mathbf{u}} &= \partial_t\phi_p|_{diff} + \partial_t\phi_p|_{ad},\\ \partial_t\phi_p|_{ad} &= (g^{ij}z_i\nabla_j\phi_p)\partial_t h,\end{aligned} \tag{17}$$

where z_i are the components of the vector normal to the reference plane in the direction of the tangent vectors defined by the membrane surface coordinates.

The total energy F in Eq. (2) decays as the system evolves, although not in a simple manner since the different energy contributions become dominant at different phases of the evolution. For example, the line-tension energy dominates at early times as the system phase separates into bulk phases, but decays rapidly. However, the bending energy is small initially but decays slowly and becomes more important at later phases in the evolution. As larger phase-separated domains form that are approximately able to adopt their spontaneous curvatures, the bending energy decays at a faster rate.

E. Numerical methods

In the simulation, spatial derivatives are calculated using a second-order centered-difference scheme. The size of the time step is determined to ensure numerical stability. Integration of the equations of motion for the height and composition variables is carried out using a forward Euler scheme. Orthogonal lattices consisting of 64 by 64 mesh points (selected in order to run a large quantity of simulations) are used to discretize the compositions and height on a computational domain of size 2.25 by 2.25, with periodic boundary conditions imposed on all four computational-domain boundaries. The cell size and other parameters were chosen based on previous calculations in Refs. 54 and 59, so that different morphologies are each thermodynamically favored in different regions of composition space for this system with equilibrium spontaneous curvatures of -1 and 1. Energy and length scales of the system can be set by the bending rigidity and the spontaneous curvature of preferentially interacting phases, α and δ. Specifically, we measure all energies in units of the bending rigidity $\Lambda = 1$, and all lengths in units of the radius of spontaneous curvature for the configuration when α aligns with δ, $C^{-1} = 1$. Simulations were performed using the following model parameters: $\sigma = 0.4$, $w = 113.8$, $\zeta = 0.40$, $M = 1$, and $\Gamma = 30$. Since the phase-field model employed requires a diffuse interface between coexisting phases, interfaces must be numerically resolved; thus, the parameters w and ζ are set such that a minimum of 6 spatial grid points exist across an interfacial region (i.e., over a thickness of the interface defined by $\phi_p \approx 0.1-0.9$), as well as specify a line tension of $\lambda = 0.5$. The inverse of the friction coefficient Γ is set so that the shape will follow the composition. The membrane shape is initialized to be perfectly planar ($h = 0$), and the compositions of the two leaflets are initialized with a small amplitude ($\pm 5.0 \times 10^{-2}$) of random noise added to a specified average composition, which is defined separately in each leaflet. A different random seed is used to initialize each leaflet.

III. RESULTS

By scaling arguments, when the coupling constant χ is set to a value of 1, the magnitude of the coupling energy appearing in Eq. (6) is comparable to the magnitude of the bending energy appearing in Eq. (4). Simulations were performed for $\chi = 1$, 10, and 20. To illustrate the effect of interleaflet interactions on the morphologies of bilayer systems, we have constructed morphological phase diagrams that map morphological phases for three different values of the coupling strength χ, presented in Fig. 4. Since our model accounts for kinetics as well as thermodynamics, the system can evolve to a local minimum in the free energy landscape and become trapped in this stationary state, and will not find the global minimum in the landscape without a large perturbation to push it out of the local minimum. Therefore, the results reported in the phase diagram represent our observations of what we refer to as "stationary states" reached kinetically, which are not necessarily global thermodynamic equilibrium states.

We use the term "morphological phase" to refer to the arrangement of the thermodynamic phases, where a stripe morphology indicates alternating regions of these phases with linear interfaces, and a caplet morphology indicates round, isolated domains of one phase in a matrix of the other phase.[59] These morphologies are also reported in the works of Hirose *et al.*[49] and Kumar *et al.*[50] However, the work of Kumar *et al.* focuses on the weak segregation limit, and they therefore observe additional morphologies with microsegregation characteristics. Each phase diagram is plotted in composition space, with the percentage of the α phase in leaflet 1 along the x-axis and the percentage of the γ phase in leaflet 2 along the y-axis, both in intervals of 10%. Simulations were performed at compositions along and below the diagonal running from $(\%\alpha, \%\gamma) = (0, 0)$ to (100, 100), which we will refer to as the major diagonal. The line running from $(\%\alpha, \%\gamma) = (0, 100)$ to (100, 0) will be referred to as the minor diagonal. Since the system is symmetric about the major diagonal, the simulation results are reflected onto the region above the major diagonal, and these patches are indicated with a dot pattern over the color. The term "overall composition" will be used throughout this discussion and is defined as the total fraction of the entire bilayer occupied by the pair of preferentially interacting phases, α and δ. For example, a system composed of 20% α (80% β) and 60% γ (40% δ) has an "overall composition" of $(20\% + 40\%)/2 = 30\%$. A system with an "overall composition" of 50% is termed an "overall equal" mixture, while a system with an "overall composition" of 0% or 100% is termed an "overall pure" mixture, for brevity. Here, "pure" does not indicate a system with only one lipid species, but rather a system with only one phase, which is composed of a mixture of species.

Most of the square patches in the phase diagrams represent a single simulation result, and each of these simulations were initialized using the same random seed referred to as the standard random seed. The color of each patch is determined by the result from the simulation using the standard random seed. However, for certain compositions, four simulations were performed, each initialized with a different random seed. These patches are additionally marked with a number indicating how many of those four simulations produced the same result as the one initialized with the standard random seed. For example, a dark blue patch with a number "3" indicates that the standard random seed simulation equilibrated to caplets in both leaflets, and three of four of the simulations initialized with different random seeds also equilibrated to caplets in both leaflets. If a number less than four is on a patch colored to indicate caplets (dark blue), the other

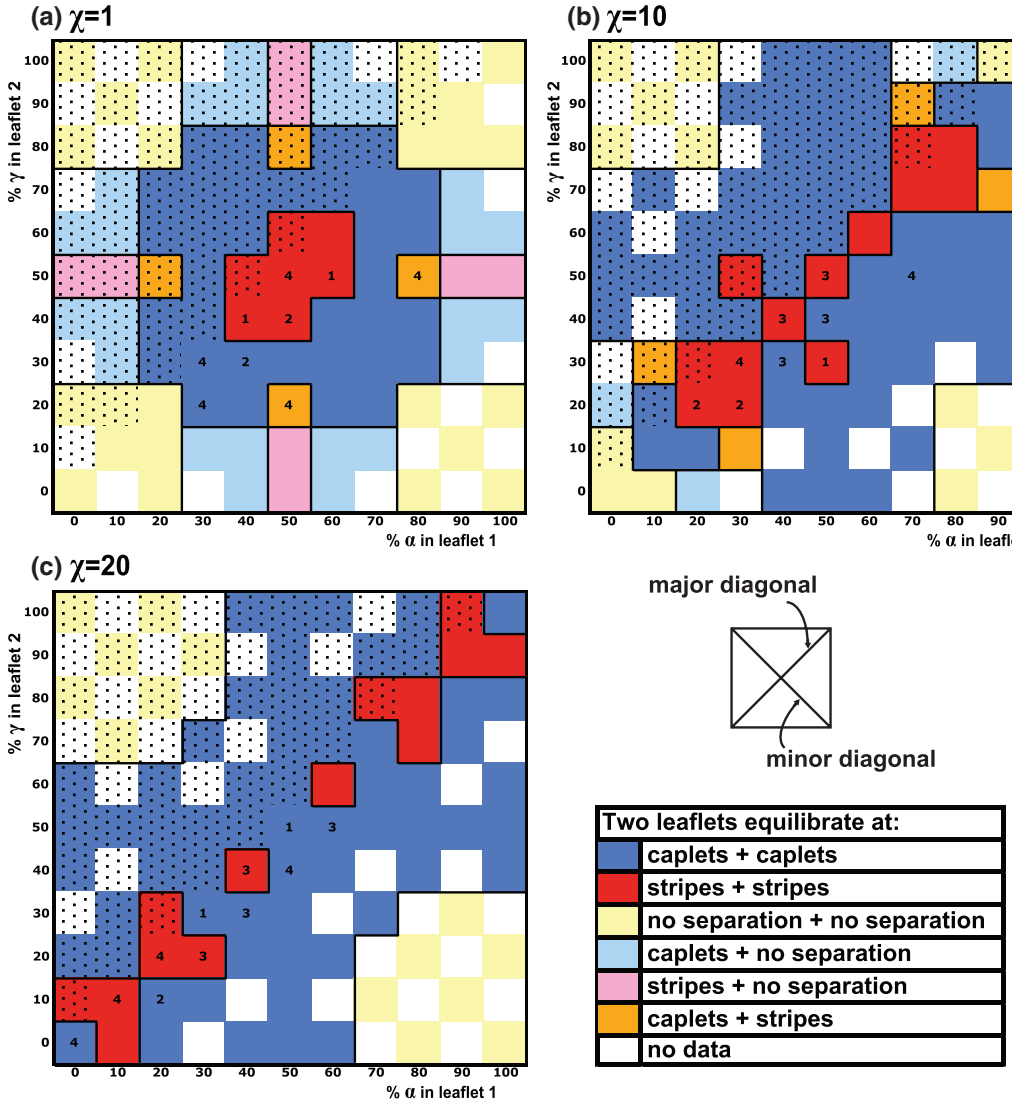

FIG. 4. Morphological phase diagrams for bilayer systems at three different interleaflet coupling strengths (weakest to strongest): (a) $\chi = 1$, (b) $\chi = 10$, and (c) $\chi = 20$. Each colored square patch along and below the major diagonal represents a simulation result; simulation results are copied to the top half (patches shown with a dot pattern). In the legend, "no separation" means the leaflet did not phase separate. The numbers indicate concentrations where four simulations using different random initializations were run; the number indicates how many of these four simulations equilibrated in the morphology represented by the color of the patch (either caplets or stripes).

morphology observed was stripes, and if a number less than four is on a patch colored to indicate stripes (red), the other morphology observed was caplets.

The phase diagrams in Fig. 4 are generally symmetric about the minor diagonal as well as the major diagonal, although this is not as clear on the $\chi = 10$ diagram in Fig. 4(b). This is because in the region in the center of the diagram, extending out along the major diagonal, the observed stationary morphologies were found to be sensitive to initial conditions, where different random seeds in the initialization would lead to different stationary states, some of which are local, not global, equilibria. In each of these simulations, either caplets or stripes were observed to be the stationary state. Where a patch shows a "4," that set of concentrations was not sensitive to initial conditions and the color is representative of the observed single morphology. On the other hand, where a patch shows a "3," three out of four different seeds produced the same (dominant) morphology as the one observed with the standard seed. A patch showing a "1" is similar, with three out of four seeds producing the same result, with the standard seed producing a different result. The patch at $\chi = 10$ and $(\%\alpha, \%\gamma) = (50, 30)$ is marked with a "1," which is the only patch that breaks the symmetry across the minor diagonal. Therefore, in a representation showing the dominant morphologies, the diagrams would all appear symmetric about both diagonals. Other patches that show a "1" run along the major diagonal in the $\chi = 20$ case, where stripes was the dominant morphology for almost the entire length of the diagonal (excluding the corner patches).

Similarities across the different coupling strengths, as observed from the diagrams in Fig. 4, include (i) the diagrams are generally symmetric about the minor diagonal as well as the major diagonal, (ii) the stripe morphology is favored when the compositions of both leaflets are near equal mixtures ($(\%\alpha, \%\gamma) \approx (50, 50)$), and (iii) no phase separation occurs when the bilayer is an "overall nearly pure"

mixture. These results are expected based on thermodynamic considerations.

However, there are also numerous differences in the results at the different coupling strengths. First, we find that stronger coupling tends to favor the stripe morphology along the length of the major diagonal, rather than just in the center of composition space. For systems where phases have equal but oppositely signed spontaneous curvatures, in the absence of interleaflet coupling, roughly equal mixtures tend to form a striped morphology while mixtures far from 50% tend to form a caplet morphology.[59] An important characteristic of the systems along the major diagonal is that they are "overall equal" mixtures. With strong coupling, the "overall composition" has a greater effect, and an "overall equal" mixture system behaves like a simple two-phase equal mixture system where the phases have mismatched spontaneous curvatures and a stripe morphology is favored. In contrast, when no shape coupling is included as in the model of Hirose *et al.*,[49] the stripe morphology is not observed for compositions at the extremes of the major diagonal, indicating that the mismatched curvature of the phases is also playing a role in favoring stripes.

The tendencies of "overall equal" mixtures (or nearly "overall equal" mixtures) to form stripes can be further understood by the detailed observation of the dynamics of the morphological evolution. When the coupling constant is larger and thus phases with preferred interactions have a stronger driving force to coincide, there are two main consequences. The first is that stronger coupling drives the system to phase-separate more quickly, with sharper (yet resolved) interfaces, as well as more precisely aligned domains. These can be observed by comparing the series of snapshots presented in Figs. 5 and 6. The second consequence of stronger coupling is that the bulk phase values of ϕ_1 and ϕ_2 shift to accommodate the stronger driving force. Since the average values of ϕ_1 and ϕ_2 remain fixed to conserve mass, the shift in bulk phase compositions is balanced by changes in the fractions of the phases. For example, consider a system with stronger coupling ($\chi = 20$) initialized with 80% α phase ($\phi_{1,avg} = 0.8$ and 20% β) and 70% γ phase ($\phi_{2,avg} = 0.7$ and 30% δ). Since the α and δ phases are present in significantly different amounts yet have a strong driving force to align, the bulk phase value for α and γ shifts in both leaflets from $\phi_{1,2} = 1$ to $\phi_{1,2} = 1.19$, forming α' and γ' phases, and for β and δ this value shifts in both leaflets from $\phi_{1,2} = 0$ to $\phi_{1,2} = 0.25$, forming β' and δ' phases. To conserve mass and maintain the average composition values of $\phi_{1,avg} = 0.8$ and $\phi_{2,avg} = 0.7$, the relative amounts of the phases shift toward 0.5. We observe in the stationary state the α' phase present at 58.5% (defined with $\phi_1 = 1.19$) and the δ' phase present at 41.5% (defined with $\phi_2 = 0.25$). These altered phase fraction values are then close enough to equal mixtures that stripes are observed in the stationary state, even though the initial phase fractions were far from equal mixtures. This observation of shifting equilibrium phase compositions is similar to the phenomena observed in asymmetric bilayers in Ref. 20, where distinct new phases appear in a phase-separated leaflet that would not be present in the absence of interactions with the opposing leaflet (i.e., in a bilayer system with uncoupled leaflets). Our simulation results provide evidence that such observations can be explained by the contribution of interleaflet interactions to the thermodynamics of the bilayer system.

Second, we find that stronger coupling favors phase separation for composition sets at the extremes of the major diagonal, where the systems are "overall equal" mixtures but the individual leaflets are nearly "pure" mixtures. With weaker coupling, the "overall composition" has a smaller effect than the individual leaflet compositions. Since there is less tendency toward spontaneous phase separation (spinodal decomposition) for nearly "pure" mixtures in general, the composition sets at the extremes of the major diagonal are only driven to phase separate with strong interleaflet coupling, and the phases tend to arrange as stripes. This can be contrasted to regions at the extremes of the minor diagonal, where phase separation is not observed at any coupling strength, since the "overall composition" and individual leaflet compositions are both nearly "pure" mixtures. While we have only investigated systems where both leaflets have the same interfacial energy parameters (constants in Eq. (3)), varying these parameters could alter the size of the regions on the phase diagrams indicating no phase separation. However, if the coupling effects are strong enough to drive phase separation in both leaflets, the "overall composition" should play as important a role as in the results we report, particularly with respect to the formation of the stripe morphology.

Lastly, we observe that stronger coupling drives both leaflets of the bilayer to adopt the same phase morphologies, as the $\chi = 20$ diagram in Fig. 4(c) is composed entirely of such states, whereas the $\chi = 1$ diagram in Fig. 4(a) shows roughly one-quarter of the composition space exhibiting phase morphologies where the two leaflets differ. Figure 7 presents a series of snapshots for one of the cases with $\chi = 1$, where, in the stationary state, one leaflet has adopted a caplet phase morphology while the other has adopted a stripe morphology (Fig. 7(d)). The resulting shape of the membrane in Fig. 7(d) is neither a caplet nor ripple, but rather a combination of the two.

IV. DISCUSSION AND CONCLUSIONS

We have presented a phase-field model for lipid bilayer membranes that couples the compositions of the two leaflets with the deformation of the membrane. We specifically examined the effects of interleaflet interactions in systems where nonzero spontaneous curvatures are energetically favorable, investigating the interplay between the compositions of each leaflet and the shape of the membrane. By mapping and contrasting phase diagrams as the interleaflet coupling strength increases, we have found that the dynamics of phase separation and stationary morphologies increasingly depend on a key parameter: an "overall composition," defined as the total fraction of the bilayer occupied by two phases that prefer to interact across the leaflets. We have found aspects of these bilayer systems that are robust and sensitive with respect to the strength of the coupling. Characteristics that are robust with varying coupling strength include (i) no spontaneous phase separation occurs in systems that are "overall (nearly) pure" mixtures and (ii) the stripe morphology is favored when both leaflets are composed of (nearly) equal mixtures. On the other

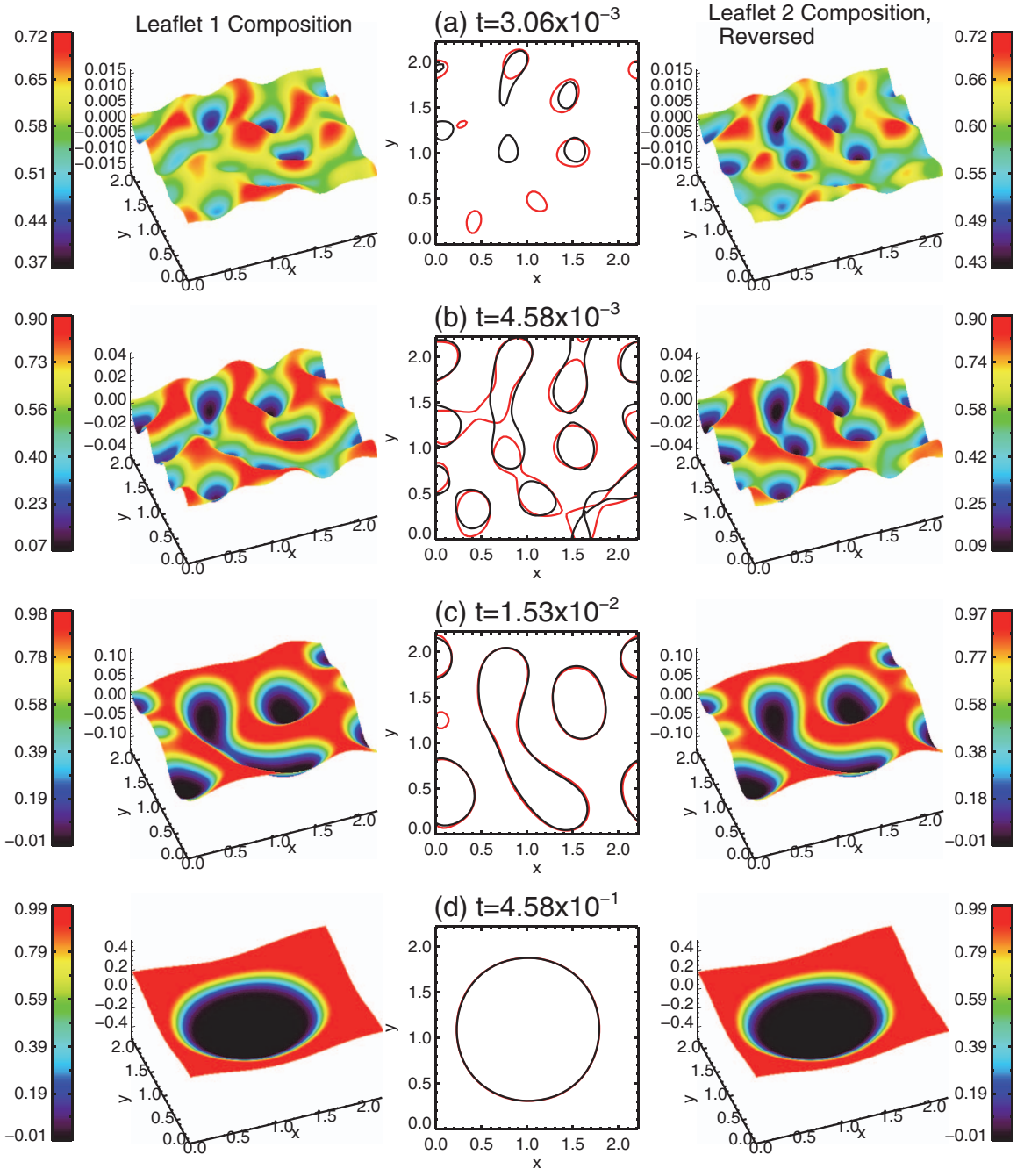

FIG. 5. Surface morphologies colored to represent the composition of a bilayer system with $\chi = 1$ and $(\%\alpha, \%\gamma) = (60, 40)$. The far left and right columns represent leaflet 1 (ϕ_1) and leaflet 2 (plotted as $1 - \phi_2$), respectively, while the center column displays contours at the phase boundaries in both leaflets to better visualize domain alignment. From top to bottom, (a) $t = 3.06 \times 10^{-3}$, (b) $t = 4.58 \times 10^{-3}$, (c) $t = 1.53 \times 10^{-2}$, and (d) $t = 4.58 \times 10^{-1}$. At early times, domains align across leaflets only roughly, but by the time a stationary state is reached they are aligned nearly precisely. This is in contrast to the system with relatively stronger coupling in Fig. 6.

hand, when comparing systems with weak coupling to those with stronger coupling we find that as the interleaflet coupling strength increases (iii) the compositions of the bulk phases and their relative amounts are increasingly altered to accommodate preferred phase alignment across leaflets, demonstrating that the strongly coupled leaflets of the bilayer form a system that appears completely different from a system with the same composition but two uncoupled leaflets; (iv) the striped morphology is increasingly preferred; (v) the phases with preferred interleaflet interactions align faster and more precisely; (vi) phase separation occurs more quickly; and (vii) the two leaflets are more likely to adopt the same phase morphology in the stationary state.

These observations indicate that as the degree of interleaflet coupling varies, membrane phase and morphological behavior also vary. To emphasize points (iii) and (iv) in the previous paragraph regarding the effect of the "overall composition" on the stripe morphology with strong coupling: We find that a system where each leaflet has a nearly "pure" mixture, which would not phase separate in the absence of

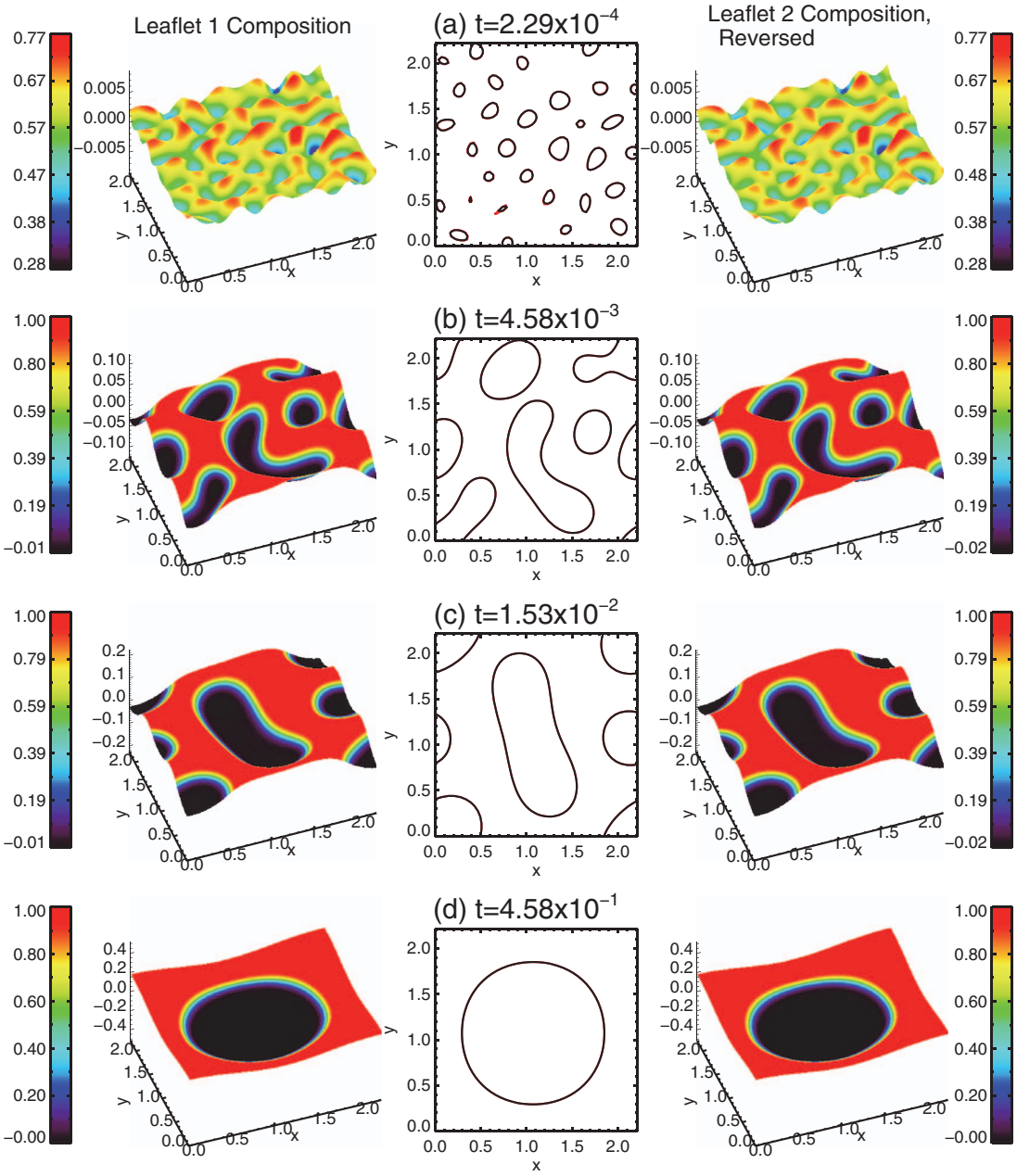

FIG. 6. Similar to Fig. 5, but for a bilayer system with $\chi = 20$ and $(\%\alpha, \%\gamma) = (60, 40)$, from top to bottom, (a) $t = 2.29 \times 10^{-4}$, (b) $t = 4.58 \times 10^{-3}$, (c) $t = 1.53 \times 10^{-2}$, and (d) $t = 4.58 \times 10^{-1}$. Even at early times, domains align across leaflets quite precisely as a result of the strong coupling between leaflets. This is in contrast to the system with relatively weak coupling in Fig. 5. Note that the earliest time shown here in part (a) is significantly earlier than the earliest time in Fig. 5(a), to further emphasize that the stronger coupling not only induces phase separation more quickly, but also aligns interfaces very quickly.

coupling, can in the presence of strong coupling not only undergo phase separation, but also significantly adjust the compositions of the phases such that it forms a nearly equal mixture with a stripe morphology. Thus the interleaflet coupling effect could be used as a tool to tune the compositions of separated membrane phases in bilayer experiments, as well as the morphologies they form. This could also be a mechanism exploited in the cell plasma membrane to control the lipid composition and arrangement of separated phases, which in turn affect membrane protein functions. Interleaflet coupling is also a potential mechanism for signal transduction across the cell plasma membrane without the involvement proteins, as the lipid environment in one leaflet can significantly alter the other leaflet. While experimental work with model systems has typically focused on symmetric membranes without examining the behavior of the individual leaflets, studies using asymmetric bilayers that probe the phase morphologies of individual leaflets of the bilayer will likely provide more information of the behavior of the (highly asymmetric) cell plasma membrane. Morphologies are also an important aspect of the behavior of asymmetric membranes, and therefore the three-dimensional morphological evolution of the membrane must be studied as well. Our model addresses both of these aspects.

In some regions of parameter space we report different results for different initializations and thus present the

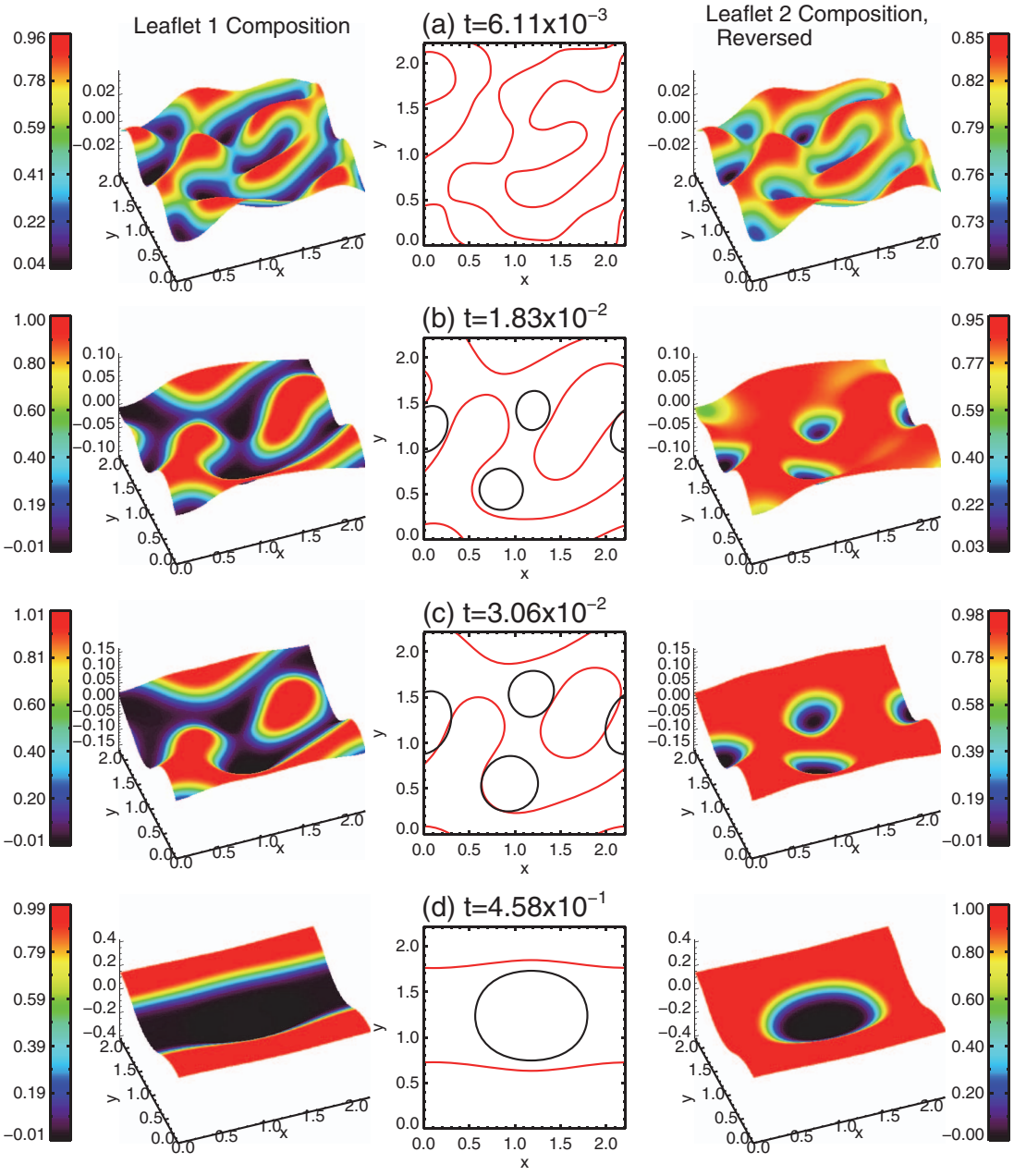

FIG. 7. Similar to Fig. 5, but for a bilayer system with $\chi = 1$ and $(\%\alpha, \%\gamma) = (50, 20)$, from top to bottom, (a) $t = 6.11 \times 10^{-3}$, (b) $t = 1.83 \times 10^{-2}$, (c) $t = 3.06 \times 10^{-2}$, and (d) $t = 4.58 \times 10^{-1}$. This case represents one of the cases where the two leaflets adopt different stationary morphologies, even though they must have the same height profile. The center plot in part (a) does not display any black interfaces since at that time leaflet 2 has not yet fully phase-separated to have the interfacial value of 0.5.

findings from multiple simulations in the phase diagrams. This sensitivity to initializations is an indication that systems with those parameters do not have a strong preference for either a caplet or stripe morphology. The periodic boundary conditions employed in this model may appear to impose an artificial numerical constraint; however, we note that real membrane systems such as lipid vesicles form closed surfaces imposing a similar constraint. For example, in order to form a stripe morphology, a phase-separated domain forms a connection with itself across the simulation cell, which is analogous to such a domain wrapping around the entire circumference of a vesicle. Additionally, the formation of a stripe morphology is less dependent on the system size for systems with "overall nearly equal" mixtures because bicontinuous-type phase morphologies form throughout the simulation cell and domains tend to span the cell, making the formation of stripes more likely. Lastly, we have ensured that the spatial resolution is sufficient to provide numerically converged results.

While outside the scope of this work, these findings could be investigated experimentally using asymmetric planar lipid bilayers composed of lipids selected for particular geometric properties, such that they would resemble the lipid schematics in Fig. 2(a). Geometric properties have been reported for various lipid species, including spontaneous curvatures, as well as how membrane curvature can be tailored with particular lipid compositions.[7,60–63] The lipids would also need to be

selected such that they would interact across the leaflets to provide a coupling energy landscape similar to that in Fig. 2(b), which could be accomplished with lipids of varying headgroup size and tailgroup length. The strength of the coupling could perhaps be varied by changing the length of the tailgroups, which would alter the degree of interdigitation and likely the strength of the interleaflet coupling.

ACKNOWLEDGMENTS

This work was supported by the UM Office of the Vice President for Research, UM startup fund, F. Solis's NSF DMR-0805330, K. Thornton's NSF DMR-0746424, and C. M. Funkhouser's NSF Graduate Research Fellowship and GAANN Fellowship on Department of Education Grant No. P200A090070. This research was also supported in part by the National Science Foundation through TeraGrid resources (now called XSEDE) provided by the Pittsburgh Supercomputing Center under Grant Nos. TG-MCB090179 and TG-DMR110007.

[1]K. Simons and E. Ikonen, Nature (London) **387**, 569 (1997).
[2]P. Sengupta, B. Baird, and D. Holowka, Semin. Cell Dev. Biol. **18**, 583 (2007).
[3]R. M. Epand, BBA-Biomembr. **1778**, 1576 (2008).
[4]L. J. Pike, J. Lipid Res. **47**, 1597 (2006).
[5]S. L. Veatch and S. L. Keller, Biophys. J. **85**, 3074 (2003).
[6]S. L. Veatch and S. L. Keller, BBA-Mol. Cell Res. **1746**, 172 (2005).
[7]K. Bacia, P. Schwille, and T. Kurzchalia, Proc. Natl. Acad. Sci. U.S.A. **102**, 3272 (2005).
[8]T. Baumgart, S. T. Hess, and W. W. Webb, Nature (London) **425**, 821 (2003).
[9]K. Jacobson, O. G. Mouritsen, and R. G. W. Anderson, Nat. Cell Biol. **9**, 7 (2007).
[10]J. Fan, M. Sammalkorpi, and M. Haataja, Phys. Rev. Lett. **100**, 178102 (2008).
[11]J. Fan, M. Sammalkorpi, and M. Haataja, Phys. Rev. E **81**, 011908 (2010).
[12]T. Baumgart, A. T. Hammond, P. Sengupta, S. T. Hess, D. A. Holowka, B. A. Baird, and W. W. Webb, Proc. Natl. Acad. Sci. U.S.A. **104**, 3165 (2007).
[13]A. Kusumi, I. Koyama-Honda, and K. Suzuki, Traffic **5**, 213 (2004).
[14]A. J. Verkleij, R. F. A. Zwaal, B. Roelofse, P. Comfuriu, D. Kastelij, and L. L. Vandeene, Biochim. Biophys. Acta **323**, 178 (1973).
[15]J. E. Rothman and J. Lenard, Science **195**, 743 (1977).
[16]P. F. Devaux, Biochemistry **30**, 1163 (1991).
[17]P. F. Devaux and A. Zachowski, Chem. Phys. Lipids **73**, 107 (1994).
[18]T. Y. Wang and J. R. Silvius, Biophys. J. **81**, 2762 (2001).
[19]C. Dietrich, L. A. Bagatolli, Z. N. Volovyk, N. L. Thompson, M. Levi, K. Jacobson, and E. Gratton, Biophys. J. **80**, 1417 (2001).
[20]M. D. Collins and S. L. Keller, Proc. Natl. Acad. Sci. U.S.A. **105**, 124 (2008).
[21]G. G. Putzel and M. Schick, Biophys. J. **94**, 869 (2008).
[22]D. W. Allender and M. Schick, Biophys. J. **91**, 2928 (2006).
[23]A. J. Wagner, S. Loew, and S. May, Biophys. J. **93**, 4268 (2007).
[24]S. Garg, J. Ruehe, K. Luedtke, R. Jordan, and C. A. Naumann, Biophys. J. **92**, 1263 (2007).
[25]C. Wan, V. Kiessling, and L. K. Tamm, Biochemistry **47**, 2190 (2008).
[26]G. G. Putzel, M. J. Uline, I. Szleifer, and M. Schick, Biophys. J. **100**, 996 (2011).
[27]H. J. Risselada and S. J. Marrink, Proc. Natl. Acad. Sci. U.S.A. **105**, 17367 (2008).
[28]W. Rodgers, B. Crise, and J. K. Rose, Mol. Cell Biol. **14**, 5384 (1994).
[29]B. Baird, E. D. Sheets, and D. Holowka, Biophys. Chem. **82**, 109 (1999).
[30]G. van Meer, Science **296**, 855 (2002).
[31]W. K. Subczynski and A. Kusumi, BBA-Biomembr. **1610**, 231 (2003).
[32]P. J. Quinn and C. Wolf, BBA-Biomembr. **1788**, 1126 (2009).
[33]M. D. Collins, Biophys. J. **94**, L32 (2008).
[34]S. May, Soft Matter **5**, 3148 (2009).
[35]M. Yanagisawa, M. Imai, T. Masui, S. Komura, and T. Ohta, Biophys. J. **92**, 115 (2007).
[36]T. S. Ursell, W. S. Klug, and R. Phillips, Proc. Natl. Acad. Sci. U.S.A. **106**, 13301 (2009).
[37]S. Semrau, T. Idema, T. Schmidt, and C. Storm, Biophys. J. **96**, 4906 (2009).
[38]J. B. Lee, P. G. Petrov, and H. Dobereiner, Langmuir **15**, 8543 (1999).
[39]L. A. Bagatolli, S. A. Sanchez, T. Hazlett, and E. Gratton, Biophotonics Methods Enzymol. **360**, 481 (2003).
[40]G. Staneva, M. I. Angelova, and K. Koumanov, Chem. Phys. Lipids **129**, 53 (2004).
[41]I. Lopez-Montero, M. Velez, and P. F. Devaux, BBA-Biomembr. **1768**, 553 (2007).
[42]E. Farge and P. F. Devaux, Biophys. J. **61**, 347 (1992).
[43]J. S. Sohn, Y.-H. Tseng, S. Li, A. Voigt, and J. S. Lowengrub, J. Comput. Phys. **229**, 119 (2010).
[44]G. S. Ayton, J. L. McWhirter, P. McMurtry, and G. A. Voth, Biophys. J. **88**, 3855 (2005).
[45]X. Wang and Q. Du, J. Math. Biol. **56**, 347 (2008).
[46]C. M. Funkhouser, F. J. Solis, and K. Thornton, Soft Matter **6**, 3462 (2010).
[47]C. Sample and A. A. Golovin, Phys. Rev. E **76**, 031925 (2007).
[48]G. Khelashvili, D. Harries, and H. Weinstein, Biophys. J. **97**, 1626 (2009).
[49]Y. Hirose, S. Komura, and D. Andelman, ChemPhysChem **10**, 2839 (2009).
[50]P. B. S. Kumar, G. Gompper, and R. Lipowsky, Phys. Rev. E **60**, 4610 (1999).
[51]M. J. Stevens, J. Am. Chem. Soc. **127**, 15330 (2005).
[52]J. B. Zhang, B. W. Jing, and S. L. Regen, Langmuir **21**, 8983 (2005).
[53]S. L. Veatch, K. Gawrisch, and S. L. Keller, Biophys. J. **90**, 4428 (2006).
[54]C. M. Funkhouser, F. J. Solis, and K. Thornton, Phys. Rev. E **76**, 011912 (2007).
[55]W. Helfrich, Z. Naturforsch. C **28**, 693 (1973).
[56]M. H. F. Wilkins, A. E. Blaurock, and D. M. Engelman, Nature New Biol. **230**, 72 (1971).
[57]S. Tristram-Nagle and J. F. Nagle, Chem. Phys. Lipids **127**, 3 (2004).
[58]R. Capovilla and J. Guven, J. Phys. A **37**, 5983 (2004).
[59]W. T. Góźdź and G. Gompper, Europhys. Lett. **55**, 587 (2001).
[60]J. Zimmerberg and M. M. Kozlov, Nat. Rev. Mol. Cell Biol. **7**, 9 (2006).
[61]E. E. Kooijman, V. Chupin, N. L. Fuller, M. M. Kozlov, B. de Kruijff, K. N. J. Burger, and P. R. Rand, Biochemistry **44**, 2097 (2005).
[62]M. E. Haque and B. R. Lentz, Biochemistry **43**, 3507 (2004).
[63]N. Fuller and R. P. Rand, Biophys. J. **81**, 243 (2001).